

# Nonreciprocal Current-induced Zero-Resistance State in Valley-Polarized Superconductors

Akito Daido,<sup>1,2,\*</sup> Youichi Yanase,<sup>1</sup> and Kam Tuen Law<sup>2</sup>

<sup>1</sup>*Department of Physics, Graduate School of Science, Kyoto University, Kyoto 606-8502, Japan*

<sup>2</sup>*Department of Physics, Hong Kong University of Science and Technology, Clear Water Bay, Hong Kong, China*

(Dated: April 18, 2025)

The recently observed nonreciprocal current-induced zero-resistance state (CIZRS) in twisted trilayer graphene/WSe<sub>2</sub> heterostructure has posed a significant theoretical challenge. Therein, the system shows a zero-resistance state only when a sufficiently large current is applied in a particular direction, while stays in an incipient superconducting state with small resistance when the current is small or in the opposite direction. In this Letter, we provide a theory for this phenomenon using a model that encapsulates valley polarization and trigonal warping inherent to the trilayer graphene/WSe<sub>2</sub> heterostructure. We elucidate that threefold-degenerate Fulde-Ferrell (FF) states are stabilized, and establish the thermodynamic phase diagram in electric current that manifests the switching behavior of different FF states. We thereby propose a scenario that predicts CIZRS in the presence of domains of different FF states: The incipient superconducting state in small current is naturally understood as a multi-domain state, wherein the inter-domain supercurrent is difficult to flow due to the tiny Josephson coupling caused by the mismatch of Cooper-pair momenta. Nevertheless, a sufficiently large current in a particular direction can selectively populate a certain FF state and create mono-domain pathways with zero resistance. Crucially, due to the threefold symmetry of the system, a current flowing in the opposite direction fails to generate these zero-resistance pathways, thus giving rise to the observed nonreciprocity. Finally, we suggest that the long-sought-after triangular finite-momentum state can also be realized in valley-polarized superconductors.

*Introduction.* — Controlling quantum states by electric currents is one of the most intriguing issues in condensed matter physics. Among various systems, superconductors offer a fascinating platform owing to their unique electromagnetic properties. It is widely believed that superconductors show zero resistance when probed with a sufficiently small current, whereas a large current generally destroys it. However, contrary to this paradigm, a recent experiment on twisted trilayer graphene/WSe<sub>2</sub> heterostructures reported a surprising situation: Under small currents, the sample exhibits a finite resistance lower than its normal-state value and, remarkably, is driven into a zero-resistance state under a sufficiently large current flowing in a particular direction [1]. Moreover, when the current flows in the opposite direction, the resistance remains finite (see Fig. 5(d) for example). This nonreciprocal current-induced zero-resistance state (CIZRS) unambiguously illustrates the necessity to update our understanding of superconductors in electric current.

The nonreciprocal behavior of the CIZRS is an analogue of the nonreciprocal transport phenomenon called the superconducting diode effect (SDE) [2, 3], which was also observed in twisted trilayer graphene/WSe<sub>2</sub> with other moiré fillings and displacement fields. From symmetry viewpoints, SDE requires broken inversion and time-reversal symmetries [3], whose origin in twisted trilayer graphene/WSe<sub>2</sub> is proposed to be a spontaneous occupation imbalance of the electrons' valley degree of freedom [1, 4–6], i.e., the valley polarization [7–14]. It is natural to consider that the valley polarization plays a key role in CIZRS as well.

There have been several attempts to explain the CIZRS. As commented on in Refs. [6, 15], CIZRS could be realized if the valley polarization was sufficiently weakened by applying electric current, because it is generally disadvantageous for superconductivity. To demonstrate this idea, superconducting

instability must be studied in dissipative electric current. Recent effort along this line, however, has not succeeded to obtain CIZRS [16]. Another possible strategy to obtain CIZRS is to drive the system out of equilibrium [17], but its connection to twisted trilayer graphene/WSe<sub>2</sub> is unclear. Thus, there is no satisfactory theory explaining CIZRS in twisted trilayer graphene/WSe<sub>2</sub>.

In this Letter, we argue that not only CIZRS but also its nonreciprocal behavior can be a natural property of superconductors with valley polarization and trigonal warping of Fermi surfaces. With a minimal model, we show that trigonal warping stabilizes the Fulde-Ferrell (FF) states, i.e., finite-momentum superconductivity with a plane-wave order parameter [18]. The obtained FF states show three-fold degeneracy, and can be externally switched by taking advantage of the coupling between Cooper-pair momentum and electric current. By establishing the electric-current phase diagram of FF states, we propose a simple scenario of CIZRS by considering FF domains and weak Josephson couplings between them due to the mismatch of Cooper-pair momenta. In particular, our scenario explains three key aspects of the experiment: 1) the incipient superconducting state at zero current; 2) the CIZRS in sufficiently large current and; 3) the nonreciprocal behavior. Moreover, the *reciprocal* CIZRS and hysteresis in current-resistivity measurement are predicted. We also point out that the long-sought-after triangular finite-momentum superconducting state [19, 20], whose order parameter is a superposition of the three FF states, can be realized in valley-polarized superconductors.

*The SLS model.* — We begin with introducing a Hamiltonian which captures the symmetry and essential features of the twisted trilayer graphene/WSe<sub>2</sub> heterostructure. The Hamiltonian is  $\hat{H} = \sum_{\mathbf{k}} \mathbf{c}_{\mathbf{k}}^\dagger H_{\mathbf{k}} \mathbf{c}_{\mathbf{k}} + \hat{H}_{\text{int}}$ , where  $\mathbf{c}_{\mathbf{k}}^\dagger =$

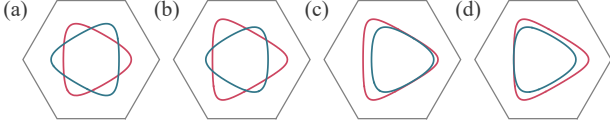


FIG. 1. (a),(b) Fermi surfaces of the SLS model for (a)  $\delta\mu = 0$  and (b)  $\delta\mu = 0.35$ . Here and hereafter, we adopt  $t = 1$ ,  $\mu = -0.65$ , and  $\phi = -0.2\pi$ . The red and blue lines indicate Fermi surfaces of the valley  $\eta = +$  and  $-$ , i.e.,  $\varepsilon_{+,\mathbf{k}} = 0$  and  $\varepsilon_{-,\mathbf{k}} = 0$ , respectively. (c),(d) Nestings of the Fermi surfaces for  $\delta\mu = 0.35$ . Red and blue curves indicate  $\varepsilon_{+,\mathbf{k}} = 0$  and  $\varepsilon_{-,\mathbf{k}+\mathbf{q}} = 0$ , respectively, with (c)  $\mathbf{q} = (0.33, 0)$  and (d)  $\mathbf{q} = (-0.19, 0)$ .

$(c_{\mathbf{k}\uparrow}^\dagger, c_{\mathbf{k}\downarrow}^\dagger, c_{\mathbf{k}\uparrow}^\dagger, c_{\mathbf{k}\downarrow}^\dagger)$  describes the electrons with spin  $s = \uparrow, \downarrow$  and valley  $\eta = \pm$ . The normal-state Bloch Hamiltonian  $H_{\mathbf{k}}$  is given by

$$H_{\mathbf{k}} = \begin{pmatrix} \varepsilon_{+,\mathbf{k}} & 0 \\ 0 & \varepsilon_{-,\mathbf{k}} \end{pmatrix} s_0, \quad \varepsilon_{\eta,\mathbf{k}} = \xi_{\eta\mathbf{k}} - \frac{\eta}{2}\delta\mu, \quad (1)$$

and  $\xi_{\mathbf{k}} = -t \sum_{n=0}^2 \cos(\mathbf{k} \cdot C_3^n \hat{x} - \phi) - \mu$ . Here,  $s_0$  represents the identity matrix in the spin space, while  $C_3$  represents the anti-clockwise three-fold rotational matrix. Thus,  $C_3^n \hat{x}$  ( $n = 0, 1, 2$ ) with  $\hat{x} = (1, 0)$  are unit vectors pointing toward the three vertices of a regular triangle, and the system accordingly has the  $C_3$  symmetry. The pairing interaction is given by  $\hat{H}_{\text{int}} = -\frac{u}{V} \sum_{\substack{\mathbf{k}\mathbf{k}'\mathbf{q} \\ s s' \eta \eta'}} c_{\mathbf{k},s\eta}^\dagger c_{-\mathbf{k}+\mathbf{q},s'\eta'}^\dagger c_{-\mathbf{k}'+\mathbf{q},s'\eta'} c_{\mathbf{k}',s\eta}$ , with the system area  $V$ , and corresponds to the onsite attractive interaction. In the following, we focus only on the inter-valley spin-singlet  $s$ -wave channel, because pairing symmetries are expected to make only quantitative changes.

This model, with some changes of notations, has been introduced by Scammell-Li-Scheurer (SLS) to discuss the intrinsic SDE in twisted trilayer graphene/WSe<sub>2</sub> [6]. Physically,  $\eta = \pm$  specifies the graphene's valley degree of freedom, and  $\mathbf{k}$  describes the wave number in the moiré Brillouin zone. Accordingly,  $\delta\mu$  describes the difference in the occupation of the valleys, namely the valley polarization [7–11]. This breaks both inversion and time-reversal symmetries, and is proposed as an origin of the observed SDE [1, 6, 21] and Josephson diode effect in gate-defined Josephson junctions in twisted bilayer graphene [22, 23]. The parameter  $\phi$  introduces the trigonal warping, which is obtained in a realistic continuum model [6]. It introduces a three-fold anisotropy as shown in Figs. 1(a) and (b). Thus, the SLS model captures the essential features of twisted trilayer graphene/WSe<sub>2</sub>, despite its simplicity.

*Finite-momentum superconductivity.* — Let us show that finite-momentum superconductivity can be realized in the SLS model. For this purpose, we introduce the pairing susceptibility

$$\chi(\mathbf{q}) = \int \frac{d^2k}{2\pi^2} \frac{1 - f(\varepsilon_{+,\mathbf{k}}) - f(\varepsilon_{-,\mathbf{k}+\mathbf{q}})}{\varepsilon_{+,\mathbf{k}} + \varepsilon_{-,\mathbf{k}+\mathbf{q}}}, \quad (2)$$

where  $f(\varepsilon) \equiv (e^{\varepsilon/T} + 1)^{-1}$  represents the Fermi distribution at temperature  $T$ . The second-order superconducting transi-

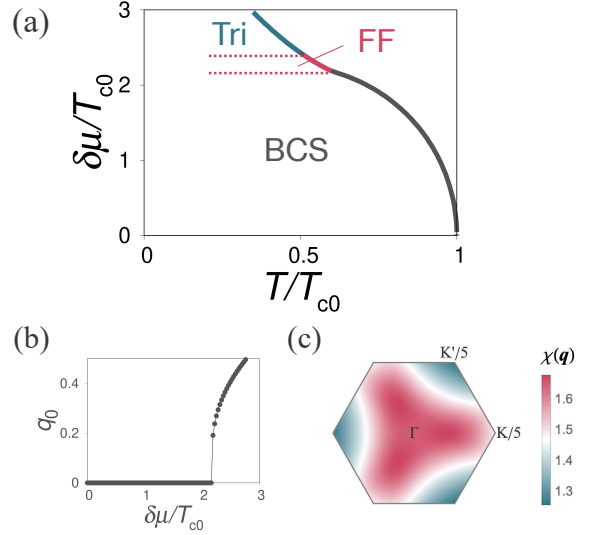


FIG. 2. (a) The  $T - \delta\mu$  phase diagram of the SLS model for  $t = 1$ ,  $\mu = -0.65$ , and  $\phi = -0.2\pi$ . We adopt  $u = 0.596$ , which gives the transition temperature  $T_{c0} \simeq 0.15$  for  $\delta\mu = 0$ . The black, red, and blue solid lines indicate the second-order phase transition from the normal state to Bardeen-Cooper-Schrieffer (BCS), Fulde-Ferrell (FF), and triangular (Tri) states, respectively. The red dotted lines are the guide for the eye. (b) Equilibrium Cooper-pair momentum along the transition line shown in panel (a). (c) Pairing susceptibility  $\chi(\mathbf{q})$  near  $\mathbf{q} = 0$  for  $\delta\mu = 0.35$  and  $T = 0.08 \simeq T_c(\delta\mu)$ .

tion takes place when  $\chi(\mathbf{q})$  exceeds the inverse of the pairing interaction  $1/u$  for a certain Cooper-pair momentum  $\mathbf{q}$ . Finite-momentum superconductivity realizes if this happens at  $\mathbf{q} \neq 0$ .

We show in Fig. 2(a) the transition line  $T = T_c(\delta\mu)$  determined by numerically solving  $1/u - \max_{\mathbf{q}} \chi(\mathbf{q}) = 0$ . The system realizes finite-momentum superconductivity when valley polarization  $\delta\mu$  exceeds a critical value  $\delta\mu_c \sim 2.2T_{c0}$  (Figs. 2(b) and (c)). According to Fig. 2(c),  $\chi(\mathbf{q})$  for  $\delta\mu \geq \delta\mu_c$  reaches its maximum at three momenta  $\mathbf{q} = \mathbf{q}_{0,1,2}$ , where

$$\mathbf{q}_0 = q_0 \hat{x}, \quad \mathbf{q}_n = C_3^n \mathbf{q}_0 \quad (n = 0, 1, 2). \quad (3)$$

This result is consistent with Ref. [6], reproducing the appearance of finite-momentum superconductivity pointed out therein. We note that Fig. 2(b) shows a jump in  $q_0$  at  $\delta\mu_c$ , implying a first-order phase transition from the Bardeen-Cooper-Schrieffer (BCS) to finite-momentum states [24].

The obtained finite-momentum superconductivity can be understood similarly to FF-Larkin-Ovchinnikov (LO) superconductors with four-fold anisotropy [25]. Generally speaking, the pairing susceptibility  $\chi(\mathbf{q})$  is maximized by the best nesting, which is achieved at  $\mathbf{q}$  parallel to  $\hat{x}$  rather than antiparallel, as in Figs. 1(c) and (d). Therefore,  $q_0 > 0$  and its  $C_3$  equivalents are favorable. The obtained critical valley polarization  $\delta\mu_c = O(T_{c0})$  is also reasonable, since the splitting of the Fermi surfaces  $\sim \delta\mu$  should exceed the Fermi-surface ambiguity  $\sim T$  coming from the Fermi distribution.

*Fulde-Ferrell and triangular states.* — We have identified the instability to finite-momentum superconductivity with three favorable momenta  $\mathbf{q}_{0,1,2}$  defined in Eq. (3). This means that when  $T$  is slightly below the transition temperature  $T_c(\delta\mu)$ , the order parameter is generally their superposition,

$$\Delta_a(\mathbf{r}) = \sum_{n=0}^2 \Delta_n e^{i\mathbf{q}_n \cdot \mathbf{r}}. \quad (4)$$

To identify the most stable combination, we substituted the ansatz Eq. (4) for the mean-field free-energy density  $F[\Delta]$ , to obtain [20, 24, 26]

$$\begin{aligned} F[\Delta_a] &= \alpha_0 (|\Delta_0|^2 + |\Delta_1|^2 + |\Delta_2|^2) \\ &+ \frac{1}{2} \beta (|\Delta_0|^2 + |\Delta_1|^2 + |\Delta_2|^2)^2 \\ &+ \beta' (|\Delta_0|^2 |\Delta_1|^2 + |\Delta_1|^2 |\Delta_2|^2 + |\Delta_2|^2 |\Delta_0|^2). \end{aligned} \quad (5)$$

This expression is ensured by  $C_3$  symmetry as well as the translational symmetry of the normal state. The first Ginzburg-Landau (GL) coefficient  $\alpha_0 \equiv 1/u - \chi(\mathbf{q}_0)$  is a small negative number, since we are focusing on  $T$  slightly below  $T_c(\delta\mu)$  where the ansatz is justified. The other GL coefficients are given by  $\beta = \beta_{00}$  and  $\beta' = 2\beta_{10} - \beta_{00}$ , with

$$\beta_{nm} = T \sum_{\omega_n} \int \frac{d^2k}{8\pi^2} \text{tr} [g_{\mathbf{k}+\mathbf{q}_n} \bar{g}_{\mathbf{k}} g_{\mathbf{k}+\mathbf{q}_m} \bar{g}_{\mathbf{k}}]. \quad (6)$$

Here, we defined the Green's functions  $g_{\mathbf{k}} = (i\omega_n - H_{\mathbf{k}})^{-1}$  and  $\bar{g}_{\mathbf{k}} = (i\omega_n + \Theta H_{-\mathbf{k}} \Theta^{-1})^{-1}$ , with Matsubara frequency  $\omega_n$  and the time-reversal operator  $\Theta$ .

The stable order parameter is determined by  $\beta'$ . In its absence,  $F[\Delta_a]$  is degenerate for all possible superpositions of  $\Delta_n$  due to  $SU(3)$  symmetry. The degeneracy is lifted by  $\beta'$ , and the FF state

$$\Delta_{\text{FF},n}(\mathbf{r}) = \Delta_n e^{i\mathbf{q}_n \cdot \mathbf{r}} \quad (n = 0, 1, 2), \quad (7)$$

is stabilized for  $\beta' > 0$  since it vanishes the  $\beta'$  term. On the other hand, the triangular state [19, 20]

$$\Delta_{\text{Tri}}(\mathbf{r}) = \sum_n \Delta_n e^{i\mathbf{q}_n \cdot \mathbf{r}}, \quad |\Delta_0| = |\Delta_1| = |\Delta_2|, \quad (8)$$

is stable for  $\beta' < 0$ , maximizing the benefit from  $\beta'$ . The other solution given by the superposition of two plane waves turns out to always have a subleading free energy [24].

We show in Fig. 3 the numerical results of the GL coefficients  $\beta$  and  $\beta'$  of the SLS model along the transition line in Fig. 2(a). We also show  $\beta'' = \beta + 2\beta'/3$ , whose positivity ensures the transition from the normal state to the triangular state to be second order [24], while  $\beta$  plays the same role for the FF state. The black and red curves for  $\beta$  and  $\beta'$ , respectively, coincide for small  $\delta\mu$  since  $q_0 = 0$  and thus  $\beta_{00} = \beta_{10}$  from Eq. (6). They split after  $\delta\mu_c$  is reached. We can see that  $\beta'$  stays positive before, and then turns negative after,  $\delta\mu \sim 2.4T_{c0} > \delta\mu_c$ , while  $\beta$  and  $\beta''$  remain positive. Thus,

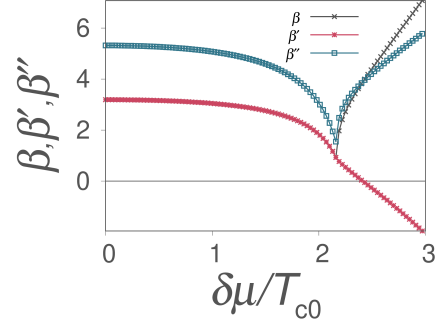


FIG. 3. The quartic Ginzburg-Landau coefficients  $\beta$ , (black)  $\beta'$ , (red) and  $\beta''$  (blue) calculated along the transition line shown in Fig. 2(a).

we obtain the phase diagram as shown in Fig. 2(a), indicating the successive transitions of BCS, FF, and the triangular states upon increasing the valley polarization  $\delta\mu$  near the transition line.

The phase diagram can be understood based on the result of the isotropic 2D system in the Zeeman field. Therein, the system experiences successive transitions of BCS, LO (indicating  $\Delta(\mathbf{r}) \sim \cos \mathbf{q} \cdot \mathbf{r}$  [26]), triangular, tetragonal, and hexagonal states, upon increasing the Zeeman field [19, 20]. By introducing the trigonal warping and breaking two-fold rotational symmetry, LO, tetragonal, and hexagonal states become unstable, while the triangular state should remain. Furthermore, the FF state may take the position of the LO state for small time-reversal breaking field: Indeed, FF state is known to appear nearby the LO state in disordered  $d$ -wave superconductors [27]. In this way, the trigonal anisotropy and valley polarization stabilize the FF and triangular states, giving exception to the common belief that LO state is stable in most cases.

*Current phase diagram of the FF states.* — In the following, we focus on the parameter regime where FF states are stabilized. In this case, the system has the three-fold degeneracy of the  $\mathbf{q}_{0,1,2}$  states, and the actual state realized in experiments would be determined by perturbations of intrinsic and/or extrinsic origins. Let us assume that small uniform nematicity  $\epsilon$  is introduced to the system, e.g., by nematic order and/or uniaxial strain. The free-energy density of each FF state changes from  $F_0 \equiv F[\Delta_{\text{FF},n}]$  to

$$F_n(\epsilon) = F_0 + \epsilon \chi_n^{\text{nem}}, \quad (9)$$

with a nematic susceptibility  $\chi_n^{\text{nem}}$  of the  $\mathbf{q}_n$  state. This generally lifts the three-fold degeneracy, and the state minimizing  $F_n(\epsilon)$  is realized.

Interestingly, we can externally control the energetics of FF states by using the supercurrent. When the current density  $\mathbf{j}$  is applied, the superconducting state is determined to minimize the Gibbs free-energy density [28–30]:

$$G(\epsilon, \mathbf{j}) = \min_{n=0,1,2} [F_n(\epsilon) - \mathbf{q}_n \cdot \mathbf{j} + O(j^2, \epsilon j)]. \quad (10)$$

Crucially, the momentum  $\mathbf{q}_n$  of the FF state directly couples

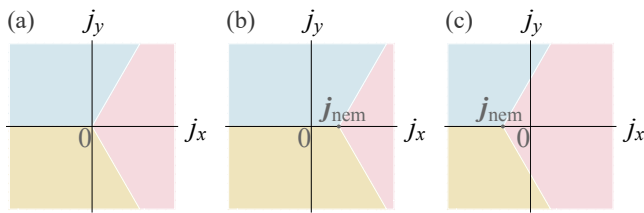


FIG. 4. Thermodynamic phase diagrams of the spatially uniform FF states in the current density  $\mathbf{j} = (j_x, j_y)$  (a) without and (b,c) with nematicity. The panels (b) and (c) correspond to the cases of  $\mathbf{j}_{\text{nem}}$  parallel and antiparallel to  $\hat{x}$ . The red, blue, and yellow regions indicate the FF states with Cooper-pair momentum  $\mathbf{q}_0$ ,  $\mathbf{q}_1$ , and  $\mathbf{q}_2$ , respectively.

to the current density  $\mathbf{j}$ , and the competition with the nematicity triggers the switching between the FF states. We show in Fig. 4(a) the  $(j_x, j_y)$  phase diagram in the absence of nematicity. Each FF state is stabilized when the current is oriented along its Cooper-pair momentum. By analyzing Eq. (10), it turns out that the nematicity just shifts the entire phase diagram by a current density  $\mathbf{j}_{\text{nem}} = O(\epsilon)$ , as discussed in End Matter. Figures 4(b) and (c) illustrate the cases where  $\mathbf{j}_{\text{nem}}$  is parallel and antiparallel to the  $x$  axis, with  $\mathbf{j}_{\text{nem}} = (j_{\text{nem}}, 0)$  and  $j_{\text{nem}} = 2(\chi_0^{\text{nem}} - \chi_1^{\text{nem}})\epsilon/3q_0$ . Note that we are focusing on the small-current regime, and the actual superconducting states would be cut off at large current due to some critical-current mechanisms. The thermodynamic  $(j_x, j_y)$  phase diagram of the trigonal FF superconductors is one of the main results of this paper.

*Current-induced zero resistance state.* — Keeping the bulk properties in mind, we point out that the switching phenomena of different FF states can naturally give rise to the CIZRS. Let us assume that the twisted trilayer graphene/WSe<sub>2</sub> heterostructure stabilizes the three-fold (near-)degenerate FF states as shown in the SLS model, and the domains of the FF states are formed after the temperature is lowered below a critical temperature. This is a reasonable assumption for twisted trilayer graphene/WSe<sub>2</sub>, because the valley polarization naturally follows from the field-trainability of SDE and spin-orbit coupling [1, 6] and  $\chi(\mathbf{q})$  with the three-peak structure has also been obtained in a realistic continuum model for essentially the same reason as in the SLS model [6]. Domains can be formed for various intrinsic and/or extrinsic reasons, including the configuration entropy and disorders in twist angle and/or local strain [31, 32].

Our scenario is based on two key observations. First, the domains between FF states of different Cooper-pair momenta would be resistive. Indeed, the Josephson energy  $E_J$  is tiny for such a situation [33, 34]. The global coherence is not achieved when the typical value of  $E_J$  is smaller than temperature and/or the charging energy, according to the Josephson-network theory [35, 36]. It is also known that vortices can be spontaneously formed at the interface of superconductors with different Cooper-pair momenta [37], whose motion may also produce dissipation. Thus, this multi-domain state is expected

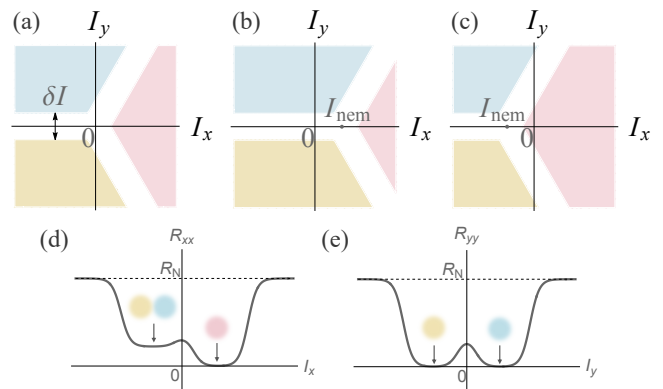


FIG. 5. (a)-(c) Schematic  $(I_x, I_y)$  phase diagrams and (d),(e) current-resistivity relation of the trigonal FF superconductors. Panels (a-c) correspond to Figs. 4 (a-c), and show the phase diagrams (a) with and (b,c) without nematicity, with a phenomenologically-introduced randomness  $\delta I$ . The white region indicates a multi-domain state, and thus is resistive. Panels (d) and (e) indicate the expected resistance in  $(I_x, 0)$  and  $(0, I_y)$  for panel (a), where  $R_N$  indicates the normal-state resistance.

to have a finite resistance lower than its normal-state value and realizes an incipient superconducting state with small resistance.

Second, the domain configuration would significantly be modified by large currents. When we apply a current  $I_x > 0$  in the  $x$  direction, the superconducting domains will switch to the  $\mathbf{q}_0$  state according to, e.g., Fig. 4(a). The realized mono-domain state would be dissipationless when zero resistance paths are formed. On the other hand, domains of  $\mathbf{q}_1$  and  $\mathbf{q}_2$  states would remain if the current flows in the opposite direction with  $I_x < 0$ , leaving the system resistive. Thus, nonreciprocal CIZRS is obtained in trigonal FF superconductors.

We expect that the actual switching occurs in a finite current strength, in contrast to Fig. 4(a). This is because there should be some domain pinnings as well as the variation in strength and direction of the current density each domain feels. The latter can occur by the current-path meandering, which is ubiquitous in percolating superconductivity and is particularly relevant to moiré superconductors [31, 32, 38, 39]. These effects would broaden the transition lines between different FF states, and we expect the  $(I_x, I_y)$  phase diagram as in Fig. 5(a). Herein, the white region indicates multi-domain states and thus is resistive, and its width  $\delta I$  is phenomenologically introduced as a measure of randomness. The current-resistivity relation for  $I_x$  would look like Fig. 5(d), whose detailed shape can depend on the domain details, qualitatively explaining the nonreciprocal CIZRS observed in the experiment [1]. An interesting prediction is the reciprocal CIZRS as in Fig. 5(e), which is expected when a current is driven in the  $y$  direction by the switching to  $\mathbf{q}_1$  and  $\mathbf{q}_2$  states in  $I_y > 0$  and  $I_y < 0$ , respectively.

Note that bulk nematicity has been observed in twisted trilayer graphene/WSe<sub>2</sub> [1, 4, 5]. In its presence, the  $(I_x, I_y)$  phase diagram would be shifted by  $I_{\text{nem}}$ , that is, a current

scale corresponding to  $j_{\text{nem}}$ , leading to the phase diagrams as in Figs. 5(b) and (c). Interestingly, a substantial SDE with a mono-domain configuration is expected instead of the CIZRS for  $I_{\text{nem}} \lesssim \delta I$  as in Fig. 5(c). This is consistent with the experiment [1], where both huge SDE and CIZRS have been observed depending on the moiré filling and displacement field. Such a state naturally accompanies a significant anisotropy in the critical current, which also agrees with a recent experiment [40].

So far, we have assumed that each domain obeys the thermodynamic phase diagram given in Fig. 4. On the other hand, the transitions between different FF states are first order, and thus hysteresis can appear depending on how the current is swept in experiments. When the current is reduced from a large value, e.g., in the positive  $x$  direction, the sample can remain in the  $q_0$  state beyond the thermodynamic phase boundary. We expect that this is related to the observed vanishing nonreciprocity and CIZRS when the sample was in a large current before the resistivity is measured [1]. More direct observation of the hysteresis in the current-resistivity relation, as well as the reciprocal CIZRS as in Fig. 5(e), will give strong supporting evidence of our scenario.

*Discussion.* — While we have concentrated on FF states (Eq. (7)), the long-sought-after triangular state (Eq. (8)) [19, 20] is predicted to exist nearby according to the free energy analysis. Thus, valley-polarized superconductors offer a promising field-free platform for its observation. Considering its closeness to the FF states in the phase space, it could be accessible in twisted trilayer graphene/WSe<sub>2</sub> by tuning parameters. Being a honeycomb lattice of vortices and antivortices [41], the triangular state would be observable e.g., by scanning-tunneling microscopy and superconducting quantum interference devices. The triangular state does not show degeneracy except for the overall translation (see End Matter for details), and will not show nonreciprocal CIZRS. This can be used as another test bed of our scenario.

Our prediction can be generalized to the other FF superconductors with multiple degeneracy. For example, heterostructures of an Ising superconductor [42–44] and ferromagnet or others may provide alternative platforms of nonreciprocal CIZRS [24]. In contrast to nonreciprocal CIZRS, a reciprocal CIZRS can be realized in  $C_2$ -symmetric FF superconductors such as disordered  $d$ -wave superconductors [27]. Thus, it is interesting to explore this possibility in the candidate materials including CeCoIn<sub>5</sub> thin films and superlattices [45].

We appreciate fruitful discussions with J.I.A. Li. A.D. thanks Heng Wu, and Shuntaro Sumita for helpful discussions, and Kazumasa Hattori and Satoru Hayami for informing him of Ref. [41] and Refs. [46, 47]. This work was supported by JSPS KAKENHI (Grant Nos. JP18H01178, JP18H05227, JP20H05159, JP21K18145, JP22H01181, JP22H04933, JP21K13880, JP23K17353, 24H01662, 23KK0248, JP25H01249, JP24H00007, JP24K21530). K. T. L. acknowledges the support of the Ministry of Science and Technology, China, and Hong Kong Research Grant Council through Grants No. 2020YFA0309600, No. RFS2021-6S03,

No. C6025- 19G, No. AoE/P-701/20, No. 16310520, No. 16307622, and No. 16309223.

\* daido@scphys.kyoto-u.ac.jp

- [1] J.-X. Lin, P. Siriviboon, H. D. Scammell, S. Liu, D. Rhodes, K. Watanabe, T. Taniguchi, J. Hone, M. S. Scheurer, and J. I. A. Li, Zero-field superconducting diode effect in small-twist-angle trilayer graphene, *Nat. Phys.* **18**, 1221 (2022).
- [2] F. Ando, Y. Miyasaka, T. Li, J. Ishizuka, T. Arakawa, Y. Shiota, T. Moriyama, Y. Yanase, and T. Ono, Observation of superconducting diode effect, *Nature* **584**, 373 (2020).
- [3] N. Nagaosa and Y. Yanase, Nonreciprocal transport and optical phenomena in quantum materials, *Annu. Rev. Condens. Matter Phys.* **15**, 63 (2024).
- [4] N. J. Zhang, J.-X. Lin, D. V. Chichinadze, Y. Wang, K. Watanabe, T. Taniguchi, L. Fu, and J. I. A. Li, Angle-resolved transport non-reciprocity and spontaneous symmetry breaking in twisted trilayer graphene, *Nat. Mater.* **23**, 356 (2024).
- [5] P. Siriviboon, J.-X. Lin, X. Liu, H. D. Scammell, S. Liu, D. Rhodes, K. Watanabe, T. Taniguchi, J. Hone, M. S. Scheurer, and J. I. A. Li, A new flavor of correlation and superconductivity in small twist-angle trilayer graphene, arXiv [cond-mat.mes-hall] (2021), arXiv:2112.07127 [cond-mat.mes-hall].
- [6] H. D. Scammell, J. I. A. Li, and M. S. Scheurer, Theory of zero-field superconducting diode effect in twisted trilayer graphene, *2D Mater.* **9**, 025027 (2022).
- [7] P. Ajayan, P. Kim, and K. Banerjee, Two-dimensional van der waals materials, *Physics Today* **69**, 38 (2016).
- [8] K. S. Novoselov, A. Mishchenko, A. Carvalho, and A. H. Castro Neto, 2D materials and van der waals heterostructures, *Science* **353**, aac9439 (2016).
- [9] A. K. Geim and I. V. Grigorieva, Van der waals heterostructures, *Nature* **499**, 419 (2013).
- [10] K. S. Novoselov, A. K. Geim, S. V. Morozov, D. Jiang, M. I. Katsnelson, I. V. Grigorieva, S. V. Dubonos, and A. A. Firsov, Two-dimensional gas of massless dirac fermions in graphene, *Nature* **438**, 197 (2005).
- [11] K. S. Novoselov, A. K. Geim, S. V. Morozov, D. Jiang, Y. Zhang, S. V. Dubonos, I. V. Grigorieva, and A. A. Firsov, Electric field effect in atomically thin carbon films, *Science* **306**, 666 (2004).
- [12] M. Christos, S. Sachdev, and M. S. Scheurer, Correlated insulators, semimetals, and superconductivity in twisted trilayer graphene, *Phys. Rev. X* **12**, 021018 (2022).
- [13] N. Bultinck, S. Chatterjee, and M. P. Zaletel, Mechanism for anomalous hall ferromagnetism in twisted bilayer graphene, *Phys. Rev. Lett.* **124**, 166601 (2020).
- [14] Y.-H. Zhang, D. Mao, and T. Senthil, Twisted bilayer graphene aligned with hexagonal boron nitride: Anomalous hall effect and a lattice model, *Phys. Rev. Res.* **1**, 033126 (2019).
- [15] Y.-C. Zhuang and Q.-F. Sun, Current-induced re-entrant superconductivity and extreme nonreciprocal superconducting diode effect in valley-polarized systems, arXiv [cond-mat.supr-con] (2025), arXiv:2501.00835 [cond-mat.supr-con].
- [16] S. Banerjee and M. S. Scheurer, Dissipation-enhanced non-reciprocal superconductivity: application to multi-valley superconductors, arXiv [cond-mat.supr-con] (2025), arXiv:2501.01501 [cond-mat.supr-con].
- [17] A. Daido and Y. Yanase, Unidirectional superconductivity and superconducting diode effect induced by dissipation, *Phys. Rev.*

- B. **111**, L020508 (2025).
- [18] P. Fulde and R. A. Ferrell, Superconductivity in a strong spin-exchange field, *Phys. Rev.* **135**, A550 (1964).
- [19] Y. Matsuda and H. Shimahara, Fulde-ferrell-larkin-ovchinnikov state in heavy fermion superconductors, *J. Phys. Soc. Jpn.* **76**, 051005 (2007).
- [20] H. Shimahara, Structure of the fulde-ferrell-larkin-ovchinnikov state in two-dimensional superconductors, *J. Phys. Soc. Jpn.* **67**, 736 (1998).
- [21] S. Banerjee and M. S. Scheurer, Enhanced superconducting diode effect due to coexisting phases, *Phys. Rev. Lett.* **132**, 046003 (2024).
- [22] J. Díez-Mérida, A. Díez-Carlón, S. Y. Yang, Y.-M. Xie, X.-J. Gao, J. Senior, K. Watanabe, T. Taniguchi, X. Lu, A. P. Higginbotham, K. T. Law, and D. K. Efetov, Symmetry-broken josephson junctions and superconducting diodes in magic-angle twisted bilayer graphene, *Nat. Commun.* **14**, 2396 (2023).
- [23] J.-X. Hu, Z.-T. Sun, Y.-M. Xie, and K. T. Law, Josephson diode effect induced by valley polarization in twisted bilayer graphene, *Phys. Rev. Lett.* **130**, 266003 (2023).
- [24] See Supplemental Material for more details, which includes Refs. [46–48].
- [25] H. Shimahara, Enhancement of the upper critical field due to a fermi-surface effect in quasi-two-dimensional superconductors in parallel magnetic fields, *J. Phys. Soc. Jpn.* **68**, 3069 (1999).
- [26] A. I. Larkin and Y. N. Ovchinnikov, Nonuniform state of superconductors, *Zh. Eksperim. i Teor. Fiz.* **47**, 1136 (1964).
- [27] D. F. Agterberg and K. Yang, The effect of impurities on fulde-ferrell-larkin-ovchinnikov superconductors, *J. Phys. Condens. Matter* **13**, 9259 (2001).
- [28] D. E. McCumber, Intrinsic resistive transition in thin superconducting wires driven from current sources, *Phys. Rev.* **172**, 427 (1968).
- [29] K. V. Samokhin and B. P. Truong, Current-carrying states in fulde-ferrell-larkin-ovchinnikov superconductors, *Phys. Rev. B Condens. Matter* **96**, 214501 (2017).
- [30] M. Tinkham, *Introduction to Superconductivity* (Courier Corporation, 2004).
- [31] A. Uri, S. Grover, Y. Cao, J. A. Crosse, K. Bagani, D. Rodan-Legrain, Y. Myasoedov, K. Watanabe, T. Taniguchi, P. Moon, M. Koshino, P. Jarillo-Herrero, and E. Zeldov, Mapping the twist-angle disorder and landau levels in magic-angle graphene, *Nature* **581**, 47 (2020).
- [32] C. N. Lau, M. W. Bockrath, K. F. Mak, and F. Zhang, Reproducibility in the fabrication and physics of moiré materials, *Nature* **602**, 41 (2022).
- [33] K. Yang and D. F. Agterberg, Josephson effect in fulde-ferrell-larkin-ovchinnikov superconductors, *Phys. Rev. Lett.* **84**, 4970 (2000).
- [34] R. P. Kaur, D. F. Agterberg, and M. Sigrist, Helical vortex phase in the noncentrosymmetric CePt3Si, *Phys. Rev. Lett.* **94**, 137002 (2005).
- [35] I. S. Beloborodov, A. V. Lopatin, V. M. Vinokur, and D. K. Efetov, Granular electronic systems, *Rev. Mod. Phys.* **79**, 469 (2007).
- [36] A. Kapitulnik, S. A. Kivelson, and B. Spivak, Colloquium: Anomalous metals: Failed superconductors, *Rev. Mod. Phys.* **91**, 011002 (2019).
- [37] K. Aoyama and M. Sigrist, Model for magnetic flux patterns induced by the influence of in-plane magnetic fields on spatially inhomogeneous superconducting interfaces of LaAlO<sub>3</sub>-SrTiO<sub>3</sub> bilayers, *Phys. Rev. Lett.* **109**, 237007 (2012).
- [38] M. Yankowitz, S. Chen, H. Polshyn, Y. Zhang, K. Watanabe, T. Taniguchi, D. Graf, A. F. Young, and C. R. Dean, Tuning superconductivity in twisted bilayer graphene, *Science* **363**, 1059 (2019).
- [39] L. Balents, C. R. Dean, D. K. Efetov, and A. F. Young, Superconductivity and strong correlations in moiré flat bands, *Nat. Phys.* **16**, 725 (2020).
- [40] N. J. Zhang, P. A. Nosov, O. E. Sommer, Y. Wang, K. Watanabe, T. Taniguchi, E. Khalaf, and J. I. A. Li, Angular interplay of nematicity, superconductivity, and strange metallicity in a moiré flat band, arXiv [cond-mat.mes-hall] (2025), 2503.15767.
- [41] D. F. Agterberg, M. Geracie, and H. Tsunetsugu, Conventional and charge-six superfluids from melting hexagonal fulde-ferrell-larkin-ovchinnikov phases in two dimensions, *Phys. Rev. B* **84**, 014513 (2011).
- [42] X. Xi, Z. Wang, W. Zhao, J.-H. Park, K. T. Law, H. Berger, L. Forró, J. Shan, and K. F. Mak, Ising pairing in superconducting NbSe<sub>2</sub> atomic layers, *Nat. Phys.* **12**, 139 (2015).
- [43] J. M. Lu, O. Zheliuk, I. Leermakers, N. F. Q. Yuan, U. Zeitler, K. T. Law, and J. T. Ye, Evidence for two-dimensional ising superconductivity in gated MoS<sub>2</sub>, *Science* **350**, 1353 (2015).
- [44] Y. Saito, Y. Nakamura, M. S. Bahramy, Y. Kohama, J. Ye, Y. Kasahara, Y. Nakagawa, M. Onga, M. Tokunaga, T. Nojima, Y. Yanase, and Y. Iwasa, Superconductivity protected by spin-valley locking in ion-gated MoS<sub>2</sub>, *Nat. Phys.* **12**, 144 (2015).
- [45] M. Naritsuka, T. Terashima, and Y. Matsuda, Controlling unconventional superconductivity in artificially engineered f-electron kondo superlattices, *J. Phys. Condens. Matter* **33**, 273001 (2021).
- [46] S. Hayami, Y. Yanagi, and H. Kusunose, Spontaneous antisymmetric spin splitting in noncollinear antiferromagnets without spin-orbit coupling, *Phys. Rev. B* **101**, 220403 (2020).
- [47] S. Hayami, Y. Yanagi, and H. Kusunose, Bottom-up design of spin-split and reshaped electronic band structures in antiferromagnets without spin-orbit coupling: Procedure on the basis of augmented multipoles, *Phys. Rev. B* **102**, 144441 (2020).
- [48] S. K. Das and B. Roy, From local to emergent altermagnetism: Footprints of free fermions band topology, arXiv [cond-mat.mes-hall] (2024), arXiv:2403.14620 [cond-mat.mes-hall].

## End Matter

*Current phase diagram of the FF states.* — Assuming the Fulde-Ferrell order parameter, the Ginzburg-Landau (GL) free-energy density can be written as

$$F(\psi, \mathbf{q}) \equiv F[\psi e^{i\mathbf{q}\cdot\hat{\mathbf{r}}}] = \alpha(\mathbf{q})|\psi|^2 + \frac{\beta(\mathbf{q})}{2}|\psi|^4, \quad (11)$$

where  $\alpha(\mathbf{q}) = 1/u - \chi(\mathbf{q})$  and  $\beta(\mathbf{q})$  is obtained by replacing  $\mathbf{q}_0$  with  $\mathbf{q}$  in  $\beta_{00}$  defined in Eq. (6). Here,  $F[\Delta]$  is the mean-field free-energy density functional measured from that of the normal state [24]. At the transition temperature,  $\alpha(\mathbf{q})$  changes its sign at momenta  $\mathbf{q}_n \neq 0$  with  $n = 0, 1, 2$ . After optimizing the order parameter amplitude  $\psi = \psi(\mathbf{q})$ , the GL free-energy density is given by

$$F(\mathbf{q}) \equiv F(\psi(\mathbf{q}), \mathbf{q}) = \begin{cases} -\alpha(\mathbf{q})^2/2\beta(\mathbf{q}) & (\alpha(\mathbf{q}) < 0) \\ 0 & (\alpha(\mathbf{q}) \geq 0) \end{cases}. \quad (12)$$

When  $T_c(\delta\mu) - T \ll T_c(\delta\mu)$ ,  $\alpha(\mathbf{q})$  is negative only near  $\mathbf{q}_n$ . Thus, we can concentrate on the three pockets in the  $\mathbf{q}$  space

around  $\mathbf{q}_{0,1,2}$ , where the free-energy density is expanded as

$$F(\mathbf{q}_n + \delta\mathbf{q}) = F_n + \frac{1}{2} D_n^{ij} \delta q_i \delta q_j + O(\delta q^3). \quad (13)$$

Here,  $F_n = F(\mathbf{q}_n) = F[\Delta_{\text{FF},n}]$  is the free energy of the  $\mathbf{q}_n$  FF state, while  $D_n^{ij} \equiv \partial_{q_i} \partial_{q_j} F(\mathbf{q}_n)$  is its superfluid weight.

The Gibbs free energy is given by [28–30]

$$\begin{aligned} G(\mathbf{j}) &= \min_{\mathbf{q}} [F(\mathbf{q}) - \mathbf{q} \cdot \mathbf{j}] \\ &\simeq \min_{n=0,1,2} \min_{\delta\mathbf{q}} [F_n + D_n^{ij} \delta q_i \delta q_j / 2 - (\mathbf{q}_n + \delta\mathbf{q}) \cdot \mathbf{j}] \\ &= \min_{n=0,1,2} [F_n - \mathbf{q}_n \cdot \mathbf{j} - \mathbf{j}^T D_n^{-1} \mathbf{j} / 2]. \end{aligned} \quad (14)$$

In the presence of nematicity, we obtain

$$G(\epsilon, \mathbf{j}) = \min_{n=0,1,2} [F_0 + \chi_n^{\text{nem}} \epsilon - \mathbf{q}_n \cdot \mathbf{j} + O(j^2, \epsilon j)], \quad (15)$$

by replacing  $F_n \rightarrow F_n(\epsilon) = F_0 + \chi_n^{\text{nem}} \epsilon$ , where the  $O(\epsilon j)$  contribution comes from the possible change of  $\mathbf{q}_n$  by  $O(\epsilon)$ .

The minimization can be performed as follows. We here consider a general nematicity and thus  $\chi_{0,1,2}^{\text{nem}}$  may take different values. By using  $\omega = e^{2\pi i/3}$ , let us introduce

$$\langle \chi \rangle \equiv (\chi_0^{\text{nem}} + \chi_1^{\text{nem}} + \chi_2^{\text{nem}}) / 3, \quad (16a)$$

$$\bar{\chi} \equiv (\chi_0^{\text{nem}} + \omega \chi_1^{\text{nem}} + \omega^2 \chi_2^{\text{nem}}) / 3, \quad (16b)$$

and

$$\bar{q}_n \equiv q_{nx} + i q_{ny} = \bar{q}_0 \omega^n, \quad \bar{j} \equiv j_x + i j_y. \quad (17)$$

Then, we can write

$$\chi_n^{\text{nem}} = \langle \chi \rangle + 2\text{Re}[\omega^n \bar{\chi}^*], \quad \mathbf{q}_n \cdot \mathbf{j} = \text{Re}[\bar{q}_n \bar{j}^*], \quad (18)$$

by using  $1 + \omega + \omega^2 = 0$ , and obtain

$$\begin{aligned} G(\epsilon, \mathbf{j}) &= \min_{n=0,1,2} [F_0 + \langle \chi \rangle \epsilon + \text{Re}[\omega^n (2\bar{\chi} \epsilon - \bar{q}_0 \bar{j}^*)]] \\ &= \min_{n=0,1,2} [F_0 + \langle \chi \rangle \epsilon - \mathbf{q}_n \cdot (\mathbf{j} - \mathbf{j}_{\text{nem}})] \\ &= G(0, \mathbf{j} - \mathbf{j}_{\text{nem}}) + \epsilon \langle \chi \rangle. \end{aligned} \quad (19)$$

Thus, the minimization problem recasts to that of  $\epsilon = 0$ , with the shift in the  $(j_x, j_y)$  phase diagram by

$$\mathbf{j}_{\text{nem}} = 2\epsilon (\text{Re}[\bar{\chi} / \bar{q}_0^*], \text{Im}[\bar{\chi} / \bar{q}_0^*]). \quad (20)$$

This conclusion applies to any trigonal FF superconductors beyond the SLS model.

Note that the SLS model preserves the  $y$ -mirror plane  $M_y$  due to its simpleness. When the nematicity  $\epsilon$  preserves the  $M_y$  symmetry, which corresponds, e.g., to the uniaxial strain in the  $x$  direction, we obtain  $\chi_1^{\text{nem}} = \chi_2^{\text{nem}}$  and  $\bar{\chi} = (\chi_0^{\text{nem}} - \chi_1^{\text{nem}}) / 3$ , to reproduce  $\mathbf{j}_{\text{nem}}$  in the main text by using  $\bar{q}_0 = q_0$ . The minimization of  $G(0, \mathbf{j})$  is then performed by

$$\begin{aligned} G(0, \mathbf{j}) &= F_0 + \min_{n=0,1,2} \text{Re}[-\bar{q}_0 \omega^n \bar{j}^*] \\ &= F_0 + \min_{n=0,1,2} \left[ -q_0 j \cos \left( \frac{2\pi n}{3} - \theta \right) \right], \end{aligned} \quad (21)$$

with  $\bar{j} \equiv j e^{i\theta}$  and  $j \geq 0$ . This clearly indicates the phase diagram as in the main text when  $q_0 > 0$ .

*Degeneracy of the triangular state.* — We briefly discuss the degeneracy of the triangular state. Generally, the triangular state can be parametrized as

$$\Delta_{\text{Tri}}(\mathbf{r}) = |\Delta_0| \sum_{n=0,1,2} e^{i\mathbf{q}_n \cdot \mathbf{r} + i\varphi_n}. \quad (22)$$

Let us introduce  $\langle \varphi \rangle = (\varphi_0 + \varphi_1 + \varphi_2) / 3$  and  $\bar{\varphi} \equiv (\varphi_0 + \omega \varphi_1 + \omega^2 \varphi_2) / 3$ . Then, we obtain

$$\begin{aligned} \varphi_n &= \langle \varphi \rangle + 2\text{Re}[\omega^n \bar{\varphi}^*] \\ &= \langle \varphi \rangle + \text{Re}[\bar{q}_n (2\bar{\varphi} / \bar{q}_0^*)^*] \\ &= \langle \varphi \rangle - \mathbf{q}_n \cdot \mathbf{r}_\varphi, \end{aligned} \quad (23)$$

with

$$\mathbf{r}_\varphi \equiv -(\text{Re}[2\bar{\varphi} / \bar{q}_0^*], \text{Im}[2\bar{\varphi} / \bar{q}_0^*]). \quad (24)$$

Therefore, an arbitrary triangular state is written in the form

$$\Delta_{\text{Tri}}(\mathbf{r}) = |\Delta_0| e^{i\langle \varphi \rangle} \sum_{n=0,1,2} e^{i\mathbf{q}_n \cdot (\mathbf{r} - \mathbf{r}_\varphi)}. \quad (25)$$

This means that the triangular state is not degenerate except for the overall phase and the choice of the origin, similarly to the LO state in systems with two-fold anisotropy.

## Supplemental Material

### Derivation of the free-energy density

We start from the mean-field Hamiltonian

$$\hat{H}_{\text{mf}} = \frac{1}{2} \Psi^\dagger H_{\text{BdG}} \Psi + E_0. \quad (26)$$

Here, we defined the Nambu spinor  $\Psi^\dagger = (\mathbf{c}^\dagger, \mathbf{c}^T U_\Theta)$ , the creation operator of electrons at position  $\mathbf{R}$  and internal degrees of freedom (spin and valley)  $a$  by  $[\mathbf{c}^\dagger]_{\mathbf{R},a} = c_a^\dagger(\mathbf{R})$ , and the unitary part of the time-reversal operator  $U_\Theta = i s_y \eta_x$ , where  $s_i$  and  $\eta_i$  are the Pauli matrices in the spin and valley spaces. The Bogoliubov-de-Gennes (BdG) Hamiltonian is given by

$$H_{\text{BdG}} = \begin{pmatrix} H & \Delta \\ \Delta^\dagger & -\Theta H \Theta^{-1} \end{pmatrix}, \quad (27)$$

where  $\Theta = U_\Theta K$  and  $K$  represents the complex conjugation operator. The constant  $E_0$  for the SLS model is given by

$$E_0 = \frac{1}{4u} \text{Tr} [\Delta^\dagger \Delta] + \frac{1}{2} \text{Tr} [H], \quad (28)$$

where  $\text{Tr} [\cdot]$  runs over all the degrees of freedom including internal ones and the real-space coordinates. The order parameter has the form

$$\Delta = \sum_{\mathbf{q}} e^{i\mathbf{q} \cdot \hat{\mathbf{r}}} \Delta_{\mathbf{q}}. \quad (29)$$

Here,  $\Delta_{\mathbf{q}}$  is just a scalar since the spin-singlet inter-valley  $s$ -wave order parameter is considered. The position operator  $\hat{\mathbf{r}}$  acts like  $[\mathbf{c}^\dagger e^{i\mathbf{q} \cdot \hat{\mathbf{r}}}]_{\mathbf{R},a} = c_a^\dagger(\mathbf{R}) e^{i\mathbf{q} \cdot (\mathbf{R} + \mathbf{r}_a)}$ , where  $\mathbf{R} + \mathbf{r}_a$  is the real-space position of the  $(\mathbf{R}, a)$  electron. We have  $\mathbf{r}_a = 0$  for the SLS model.

The mean-field free energy is given by

$$\Omega[\Delta] = E_0 - \frac{T}{2} \sum_{\omega_n} e^{i\omega_n(+0)} \text{Tr}' \ln G^{-1}(i\omega_n), \quad (30)$$

with  $G^{-1}(i\omega_n) = i\omega_n - H_{\text{BdG}}$ . Here,  $\text{Tr}'$  represents the trace over the Nambu degree of freedom as well as those of the normal state. In the following, we abbreviate the argument  $i\omega_n$  when it is unnecessary. Let us define

$$\hat{G}_0 \equiv \begin{pmatrix} g & 0 \\ 0 & \bar{g} \end{pmatrix}, \quad \hat{\Delta} = \begin{pmatrix} 0 & \Delta \\ \Delta^\dagger & 0 \end{pmatrix}, \quad (31)$$

by using the electron and hole Green's function  $g = (i\omega_n - H)^{-1}$  and  $\bar{g} = (i\omega_n + \Theta H \Theta^{-1})^{-1}$ . According to the Dyson equation  $G^{-1} = \hat{G}_0^{-1} (1 - \hat{G}_0 \hat{\Delta})$ , we obtain the Ginzburg-

Landau expansion

$$\begin{aligned} \Omega[\Delta] - \Omega[0] &= \frac{1}{4u} \text{Tr} [\Delta^\dagger \Delta] - \frac{T}{2} \sum_{\omega_n} e^{i\omega_n(+0)} \text{Tr}' \ln(1 - \hat{G}_0 \hat{\Delta}) \\ &= \frac{1}{4u} \text{Tr} [\Delta^\dagger \Delta] + \frac{T}{4} \sum_{\omega_n} \text{Tr}' [(\hat{G}_0 \hat{\Delta})^2] \\ &\quad + \frac{T}{8} \sum_{\omega_n} \text{Tr}' [(\hat{G}_0 \hat{\Delta})^4] + O(\Delta^6) \\ &\equiv V(F_2[\Delta] + F_4[\Delta]) + O(\Delta^6). \end{aligned} \quad (32)$$

We defined the  $O(\Delta^2)$  and  $O(\Delta^4)$  terms as  $F_2[\Delta]$  and  $F_4[\Delta]$ , respectively, with the system area  $V$ . The superconducting contribution to the total free energy density is then given by

$$F[\Delta] = F_2[\Delta] + F_4[\Delta], \quad (33)$$

neglecting the  $O(\Delta^6)$  contribution. This is sufficient for our purpose since we are interested in the second-order superconducting transition. By taking the trace over the Nambu degree's of freedom, the traces in  $F_2[\Delta]$  and  $F_4[\Delta]$  are evaluated as follows:

$$\frac{T}{4} \sum_{\omega_n} \text{Tr}' [(\hat{G}_0 \hat{\Delta})^2] = \frac{T}{2} \sum_{\omega_n} \text{Tr} [g \Delta \bar{g} \Delta^\dagger], \quad (34)$$

and

$$\frac{T}{8} \sum_{\omega_n} \text{Tr}' [(\hat{G}_0 \hat{\Delta})^4] = \frac{T}{4} \sum_{\omega_n} \text{Tr} [(g \Delta \bar{g} \Delta^\dagger)^2]. \quad (35)$$

### $O(\Delta^2)$ term and finite-momentum superconductivity

We first discuss the  $F_2[\Delta]$  contribution. The second-order superconducting transition occurs when this contribution turns negative for some  $\Delta$ . Assuming the translational symmetry of the normal state, we obtain

$$\begin{aligned} F_2[\Delta] &= \sum_{\mathbf{q}} \frac{|\Delta_{\mathbf{q}}|^2}{V} \left[ \frac{1}{4u} \text{Tr}_{\text{N1}} + \frac{T}{2} \sum_{\omega_n} \text{Tr} [g e^{i\mathbf{q} \cdot \hat{\mathbf{r}}} \bar{g} e^{-i\mathbf{q} \cdot \hat{\mathbf{r}}}] \right] \\ &\equiv \sum_{\mathbf{q}} \alpha(\mathbf{q}) |\Delta_{\mathbf{q}}|^2. \end{aligned} \quad (36)$$

Here,  $\alpha(\mathbf{q})$  is given by  $\alpha(\mathbf{q}) = 1/u - \chi(\mathbf{q})$ , with

$$\begin{aligned} \chi(\mathbf{q}) &= -\frac{T}{2V} \sum_{\omega_n} \text{Tr} [g e^{i\mathbf{q} \cdot \hat{\mathbf{r}}} \bar{g} e^{-i\mathbf{q} \cdot \hat{\mathbf{r}}}] \\ &= -\frac{T}{2V} \sum_{\mathbf{k}, \omega_n} \text{tr} [g_{\mathbf{k}+\mathbf{q}} \bar{g}_{\mathbf{k}}]. \end{aligned} \quad (37)$$

Here,  $\text{tr}$  runs over the internal degrees of freedom, i.e., the spin and valley. We obtain  $\chi(\mathbf{q})$  in the main text by taking the trace and the summation over the Matsubara frequency.



As we have seen in the main text, the leading instability is achieved at three  $\mathbf{q}$  vectors  $\mathbf{q}_n = C_3^n \mathbf{q}_0$  ( $n = 0, 1, 2$ ) in the SLS model for large  $\delta\mu$ . Cooper-pair momentum  $q_0$  jumps at  $\delta\mu = \delta\mu_c$ , which can be understood based on the GL theory with phenomenologically assuming the validity of gradient expansion. According to the  $C_3$  and  $M_y$  symmetry, the GL coefficient  $\alpha(\mathbf{q})$  takes the form

$$\alpha(\mathbf{q}) = \alpha_0 + \frac{\alpha_2}{2} \mathbf{q}^2 + \frac{2\alpha_3}{3} (q_x^3 - 3q_x q_y^2) + \frac{\alpha_4}{4} \mathbf{q}^4, \quad (38)$$

up to  $O(q^4)$ . In contrast to the conventional FFLO states, the transition to the finite-momentum superconductivity takes place by the increase of  $|\alpha_3|$  instead of sign reversal of  $\alpha_2$ , leading to the jump of  $q_0$ . To see this, let us focus on the  $q_y = 0$  line. We obtain

$$\alpha(q_x) = \frac{\alpha_2}{2} q_x^2 + \frac{2\alpha_3}{3} q_x^3 + \frac{1}{4} q_x^4. \quad (39)$$

Here,  $\alpha_0$  is abbreviated since it does not affect the results. We also assumed  $\alpha_4 > 0$ , and set it to unity by rescaling the momentum as well as  $\alpha_2$  and  $\alpha_3$ . The extrema are obtained by

$$0 = \alpha'(q_x) = q_x(\alpha_2 + 2\alpha_3 q_x + q_x^2), \quad (40)$$

which has solutions other than  $q_x = 0$  at

$$q_x = q_{\pm} \equiv -\alpha_3 \pm \sqrt{\alpha_3^2 - \alpha_2}, \quad (41)$$

when  $\alpha_3^2 > \alpha_2$ . The value of  $\alpha(q_x)$  for these solutions are

$$\alpha(q_{\pm}) = \frac{\alpha_3^2}{12} q_{\pm}^2 (1 \pm 3 \operatorname{sgn}[\alpha_3] D) (1 \mp \operatorname{sgn}[\alpha_3] D), \quad (42)$$

with  $D = \sqrt{1 - \alpha_2/\alpha_3^2}$ . Either of  $\alpha(q_{\pm})$  is smaller than  $\alpha(0) = 0$  when

$$\alpha_3^2 > \frac{9}{8} \alpha_2. \quad (43)$$

These results clearly indicate that first-order transition to  $q_0 \neq 0$  occurs before  $\alpha_2$  turns negative, since  $\alpha_3 = O(\delta\mu)$  and thus  $\alpha_3^2 > 0$  in the presence of valley polarization.

#### $O(\Delta^4)$ term and FF and triangular states

When we assume the second-order phase transition from the normal state to the superconducting state, only plane waves with momenta near either one of  $\mathbf{q}_n$  can appear in the solution of  $\delta F[\Delta]/\Delta^\dagger = 0$  with  $F[\Delta] < 0$ . As we approach the transition temperature from below, the ansatz

$$\Delta_a = \sum_{n=0,1,2} \Delta_n e^{i\mathbf{q}_n \cdot \hat{\mathbf{r}}}, \quad \Delta_n \in \mathbb{C}, \quad (44)$$

should be asymptotically correct. The  $O(\Delta^2)$  contribution is simply given by

$$F_2[\Delta_a] = \sum_n \alpha_0 |\Delta_n|^2, \quad (45)$$

with  $\alpha_0 = \alpha(\mathbf{q}_n)$  owing to the  $C_3$  symmetry. We are focusing on such a temperature that  $\alpha_0$  is a small negative number.

Below, we evaluate  $F_4[\Delta_a]$  to determine the stable order parameter. Substituting the ansatz for  $F_4[\Delta]$ , we obtain

$$F_4[\Delta_a] = \frac{1}{2} \sum_{\substack{m_1, m_2, n_1, n_2 \\ = 0, 1, 2}} \Delta_{m_1}^* \Delta_{m_2}^* \Delta_{n_1} \Delta_{n_2} \beta_{m_1 m_2; n_1 n_2}, \quad (46)$$

with

$$\beta_{m_1 m_2; n_1 n_2} = \frac{T}{2V} \sum_{\omega_n} \operatorname{Tr} [g e^{i\mathbf{q}_{n_1} \cdot \hat{\mathbf{r}}} \bar{g} e^{-i\mathbf{q}_{m_1} \cdot \hat{\mathbf{r}}} \cdot g e^{i\mathbf{q}_{n_2} \cdot \hat{\mathbf{r}}} \bar{g} e^{-i\mathbf{q}_{m_2} \cdot \hat{\mathbf{r}}}. \quad (47)$$

There are selection rules for  $\beta_{m_1 m_2; n_1 n_2}$ . First, according to the translational symmetry of the normal state, only combinations of  $m_1, m_2, n_1, n_2$  satisfying

$$\mathbf{q}_{m_1} + \mathbf{q}_{m_2} = \mathbf{q}_{n_1} + \mathbf{q}_{n_2}, \quad (48)$$

are allowed. Note that  $\mathbf{q}_n$  is not so large in our case that Umklapp processes do not occur. It follows that

$$\beta_a \equiv \beta_{00;00} = \beta_{11;11} = \beta_{22;22}, \quad (49a)$$

$$\begin{aligned} \beta_b &\equiv \beta_{01;01} = \beta_{10;10} = \beta_{02;02} = \beta_{20;20} \\ &= \beta_{12;12} = \beta_{21;21}, \end{aligned} \quad (49b)$$

$$\begin{aligned} \beta_c &\equiv \beta_{10;01} = \beta_{01;10} = \beta_{20;02} = \beta_{02;20} \\ &= \beta_{12;21} = \beta_{21;12}, \end{aligned} \quad (49c)$$

can be finite and the others vanish. We used the relation

$$\beta_{m_1 m_2; n_1 n_2} = \beta_{m_2 m_1; n_2 n_1}, \quad (50)$$

which follows from the cyclic property of the trace, and the constraint from the  $C_3$  symmetry

$$\beta_{m_1 m_2; n_1 n_2} = \beta_{m_1+1, m_2+1; n_1+1, n_2+1}, \quad (51)$$

where the subscripts are evaluated by modulo 3. Summing up all the contributions, we obtain

$$\begin{aligned} F_4[\Delta_a] &= \frac{\beta_a}{2} (|\Delta_0|^4 + |\Delta_1|^4 + |\Delta_2|^4) \\ &+ (\beta_b + \beta_c) (|\Delta_0|^2 |\Delta_1|^2 + |\Delta_1|^2 |\Delta_2|^2 + |\Delta_2|^2 |\Delta_0|^2). \end{aligned} \quad (52)$$

The GL coefficients are explicitly written down as

$$\beta_a = \frac{T}{2V} \sum_{\mathbf{k}, \omega_n} \operatorname{tr} [g_{\mathbf{k}+\mathbf{q}_0} \bar{g}_{\mathbf{k}} g_{\mathbf{k}+\mathbf{q}_0} \bar{g}_{\mathbf{k}}], \quad (53a)$$

$$\beta_b = \frac{T}{2V} \sum_{\mathbf{k}, \omega_n} \operatorname{tr} [g_{\mathbf{k}} \bar{g}_{\mathbf{k}-\mathbf{q}_0} g_{\mathbf{k}} \bar{g}_{\mathbf{k}-\mathbf{q}_1}], \quad (53b)$$

$$\beta_c = \frac{T}{2V} \sum_{\mathbf{k}, \omega_n} \operatorname{tr} [g_{\mathbf{k}+\mathbf{q}_0} \bar{g}_{\mathbf{k}} g_{\mathbf{k}+\mathbf{q}_1} \bar{g}_{\mathbf{k}}]. \quad (53c)$$

We can show  $\beta_b = \beta_c$  by using the antiunitary property of  $\Theta$ . Thus, we obtain

$$F_4[\Delta_a] = \frac{\beta}{2} (|\Delta_0|^2 + |\Delta_1|^2 + |\Delta_2|^2)^2 + \beta' (|\Delta_0|^2 |\Delta_1|^2 + |\Delta_1|^2 |\Delta_2|^2 + |\Delta_2|^2 |\Delta_0|^2), \quad (54)$$

with

$$\beta = \beta_a, \quad \beta' = \beta_b + \beta_c - \beta_a = 2\beta_c - \beta_a. \quad (55)$$

This reproduces the expressions in the main text, by noting that  $\beta_a = \beta_{00}$  and  $\beta_c = \beta_{10}$ . Note that we have not used the gradient expansion to obtain  $F_4[\Delta_a]$ , which could be important because the gradient expansion may not be justified for description of the first-order phase transition of the Cooper-pair momenta.

Now the minimization of  $F[\Delta_a]$  recasts to that by  $\Delta_0, \Delta_1$ , and  $\Delta_2$ . It is convenient to parametrize them as

$$(\Delta_0, \Delta_1, \Delta_2) = R(e^{i\varphi_1} \cos \theta, e^{i\varphi_2} \sin \theta \cos \phi, e^{i\varphi_3} \sin \theta \sin \phi). \quad (56)$$

We obtain

$$F[\Delta_a] = \alpha_0 R^2 + \frac{\beta}{2} R^4 + \beta' R^4 \left[ \sin^2 \theta + \sin^4 \theta \left( \frac{1}{4} \sin^2 2\phi - 1 \right) \right]. \quad (57)$$

From symmetry, we can focus on the extrema in the region  $0 \leq \theta \leq \pi/2$  and  $0 \leq \phi \leq \phi/2$ . They are given by (i)  $\theta = 0$ , (ii)  $\phi = 0, \pi/2$  with  $\theta = \pi/4$ , and (iii)  $\phi = \pi/4$  with  $\sin^2 \theta = 2/3$ . The states characterized by the conditions (i), (ii), and (iii) correspond to FF, double- $q$ , and triangular states, respectively. Here, double- $q$  state (DQ) is defined as

$$\Delta_{\text{DQ},n}(\mathbf{r}) = \sum_{m \neq n} |\Delta_m| e^{i\mathbf{q}_m \cdot \mathbf{r}}, \quad |\Delta_{n+1}| = |\Delta_{n-1}|. \quad (58)$$

The free-energy density corresponding to these states are obtained by optimizing

$$F_{\text{FF}}(R) = \alpha_0 R^2 + \frac{\beta}{2} R^4, \quad (59a)$$

$$F_{\text{DQ}}(R) = \alpha_0 R^2 + \frac{\beta + \beta'/2}{2} R^4, \quad (59b)$$

$$F_{\text{Tri}}(R) = \alpha_0 R^2 + \frac{\beta + 2\beta'/3}{2} R^4, \quad (59c)$$

in terms of  $R$ . This expression indicates that  $\beta > 0$ ,  $\beta + \beta'/2 > 0$ , and  $\beta' \equiv \beta + 2\beta'/3 > 0$  are required for the transition from the normal state to FF, DQ, and Tri states to be second order, respectively. After optimization by  $R$ , we conclude

$$F_{\text{FF}} = -\frac{\alpha_0^2}{2\beta}, \quad F_{\text{DQ}} = -\frac{\alpha_0^2}{2(\beta + \beta'/2)}, \quad (60a)$$

$$F_{\text{Tri}} = -\frac{\alpha_0^2}{2(\beta + 2\beta'/3)}, \quad (60b)$$

and therefore

$$F_{\text{FF}} < F_{\text{DQ}} < F_{\text{Tri}} \quad (\beta' > 0), \quad (61a)$$

$$F_{\text{Tri}} < F_{\text{DQ}} < F_{\text{FF}} \quad (\beta' < 0). \quad (61b)$$

### Alternative platforms of nonreciprocal CIZRS

As discussed in the main text, our prediction of CIZRS can be generalized to the other FF superconductors with multiple degeneracy. For example, it is possible to obtain an equivalent to the SLS model by considering an Ising superconductor [42–44]/ferromagnet heterostructure as is briefly discussed below. In addition to the Ising superconductor/ferromagnet heterostructures,  $f$ -wave altermagnets [48] and  $120^\circ$  antiferromagnets [46, 47] could offer platforms when sandwiched by a superconductor and a ferromagnet, since they show Fermi surfaces similar to Fig. 1(a) [46–48].

In the following, we briefly show that an equivalent of the SLS model can be obtained based on the heterostructure of an Ising superconductor and a ferromagnet. The Hamiltonian of such a system can be written as

$$\hat{H} = \sum_{\mathbf{k}} \mathbf{c}_{\mathbf{k}}^\dagger H(\mathbf{k}) \mathbf{c}_{\mathbf{k}} + \hat{H}_{\text{int}}, \quad (62)$$

with

$$H(\mathbf{k}) = E_{\mathbf{k}} + g_z(\mathbf{k}) s_z - h s_z, \quad (63)$$

where  $E_{\mathbf{k}}$ ,  $g_z(\mathbf{k})$ , and  $h$  represent the hopping energy, Ising spin-orbit coupling, and the exchange field in the  $z$  direction introduced by the proximity to the ferromagnet. Here,  $\mathbf{k}$  is the usual wave number measured from the Gamma point, and  $\xi(\mathbf{k})$  and  $g_z(\mathbf{k})$  are given by

$$E(\mathbf{k}) = -t_{\parallel} \left( \cos k_x + 2 \cos \frac{\sqrt{3}k_y}{2} \cos \frac{k_x}{2} \right) - \mu = -t_{\parallel} \sum_{n=0}^2 \cos(\mathbf{k} \cdot C_3^n \hat{x}) - \mu, \quad (64)$$

$$g_z(\mathbf{k}) = \alpha_{\text{I}} \left( \sin k_x - 2 \sin \frac{k_x}{2} \cos \frac{\sqrt{3}}{2} k_y \right) = \alpha_{\text{I}} \sum_{n=0}^2 \sin(\mathbf{k} \cdot C_3^n \hat{x}), \quad (65)$$

assuming the nearest-neighbor bonds of the triangular lattice. By rewriting

$$t_{\parallel} = t \cos \phi, \quad \alpha_{\text{I}} = -t \sin \phi, \quad \text{and} \quad h = -\delta\mu/2, \quad (66)$$

we obtain

$$H(\mathbf{k}) = -t \sum_{n=0}^2 \cos(s_z \mathbf{k} \cdot C_3^n \hat{x} - \phi) - \mu + \delta\mu s_z/2 = \begin{pmatrix} \varepsilon_{+\mathbf{k}} & 0 \\ 0 & \varepsilon_{-\mathbf{k}} \end{pmatrix}, \quad (67)$$

and thus the SLS model is realized in the spin space instead of the valley space. The pairing interaction is also equivalent by assuming the on-site attractive interaction and spin-singlet  $s$ -

wave superconductivity, and thus the phase diagram is exactly the same as that of the SLS model when the corresponding parameters are equivalent.